

Chapter 2

Super-Resolution Microscopy: Principles, Techniques, and Applications

Sinem K. Saka

Abstract

Diffraction sets a physical limit for the theoretically achievable resolution; however, it is possible to circumvent this barrier. That's what microscopists have been doing in recent years and in many ways at once, starting the era of super-resolution in light microscopy. High-resolution approaches come in various flavors, and each has specific advantages or disadvantages. For example, near-field techniques avoid the problems associated with the propagation of light by getting very close to the specimen. In the far-field, the strategies include increasing the light collecting capability, sharpening the point spread function or high-precision localization of individual fluorescent molecules. In this chapter, the major super-resolution approaches are introduced briefly, together with their pros and cons, and exemplar biological applications.

Key words Superresolution, NSOM, AFM, TIRF, STED, SIM, I⁵M, 4Pi, Localization microscopy, STORM, PALM, FPALM

1 Near-Field Techniques

Light microscopy can work in two different modes depending on how far the light is allowed to propagate: far-field light propagates through space in an unconfined manner and is the typical light in conventional microscopy, while near-field light consists of a non-propagating field that exists very close to the surface of an object, at a distance smaller than the wavelength of light used for imaging. Near-field microscopy, which is in general limited to imaging of surfaces, has attained nanoscale resolution earlier than many far-field techniques. However, it has not been able to provide an increased resolution for most common biological applications, since the biological specimen are often too thick for near-field imaging. Still, some techniques like scanning near-field optical microscopy, atomic force microscopy (AFM), and total internal reflection microscopy (TIRF) have proven to be very useful for particular questions. Hence they will be briefly discussed below.

1.1 Near-Field Scanning/Scanning Near-Field Optical Microscopy

Near-field in optics is a general term for configurations that involve illumination or detection of the specimen through an element with subwavelength (smaller than the wavelength of the light used for imaging) size, located at a subwavelength distance from the specimen. This concept allows obtaining resolution substantially below the wavelength of light, because light is not allowed to diffract after leaving the aperture. The simplest way to design a setup for near-field microscopy is to avoid using lenses. Instead, an aperture smaller than the wavelength of light is positioned very close to the surface (at a distance smaller than the wavelength itself). In such a system, resolution depends on the aperture size and the distance from the sample, but not on the wavelength.

The theory of near-field scanning optical microscopy (NSOM) was proposed by Synge in 1928 [1]. The proposal involved placing an opaque plate with a hole (aperture) of 10 nm diameter in front of a strong light source. In this configuration, he envisioned local illumination of a thin biological section, which should be closer to the hole than the diameter of the hole itself. Transmitted light was to be detected point by point by a detector. Unfortunately, as he was also aware of the technology at the time was not advanced enough to build four critical components of such a microscope [1]. First, the light sources of the time were not strong enough. Second, it was very hard to move the section in very small regular increments. Third, getting a thin biological section with a flat surface was quite difficult at the time. Finally, constructing an opaque plate with a very small hole was also quite complicated. Therefore, it took several decades to develop the technology necessary for this design. Initially, the approach was demonstrated to achieve subwavelength resolution (reaching $\lambda/60$) in near-field at the microwave spectrum [2]. Then with the development of techniques in aperture fabrication, several groups independently applied it for shorter wavelengths [hence the different abbreviations NSOM and SNOM (scanning near-field optical microscopy)] using different aperture constructions [3–6]. The “aperture” here is the nano-sized opening at the end of a metal-coated optical fiber. Although theoretically arbitrarily small apertures can be created to increase the resolution, one limiting factor is the penetration depth of light into the metal aperture, which restricts the achievable resolution to 30–50 nm [7]. Alternatively, apertureless microscopes have also appeared. The apertureless NSOM (ANSOM) uses a sharp nano-sized mechanical probe tip (similar to that of an atomic force microscope as detailed below). The tip creates a local change, for example in the effective fluorescence, when it comes close to a point in the specimen surface, and this change is detected in the far-field. Since the effect is limited to the area interacting with the probe, objects much closer than the diffraction limit are discernible [8]. With apertureless setups, it is possible to reach below 10 nm resolution [7].

Using NSOM it is possible to obtain a resolution of at least ~ 80 nm and it also allows combining optical and topographical (force-based) imaging simultaneously. To keep the distance between the probe and the sample surface constant, NSOM uses a shear-force feedback control mechanism. For that, the probe tip is let to oscillate with an amplitude of less than 1 nm. When the tip is too close to the sample, the shear forces cause a change in the oscillation, which is detected through an electronic system. However, the use of this system requires the surface to be dry. Although there are protocols for structure-preserving drying processes, this creates a problem for biological specimens and fluorophores that might need an aqueous environment for desired fluorescence effects and are subject to increased photobleaching due to direct contact with oxygen [9]. These reasons, as well as the applicability of the method only to surfaces, prevented its extensive use for biology. However, in the last decade there have been successful attempts to improve the tip-sample distance regulation in liquid [10] and various cellular structures have been imaged in aqueous medium. To name a few, fluorescently labeled plasma membranes of fibroblasts or transmembrane proteins like HLA class I molecules have been visualized with a resolution of ~ 40 nm [11]. Similarly, T-cell receptor domains and aggregates of various properties have been imaged with 50 nm resolution using quantum dots for labeling [12].

1.2 Atomic Force Microscopy

Like NSOM, AFM [13] is a scanning probe microscopy technique, in which the surface of the sample is scanned with a very fine tip. While NSOM offers a direct observation of the nanostructures, AFM can provide either direct or indirect topographical images and measurements of atomic interactions. The AFM tip is positioned with high-precision in respect to the sample and is mounted to a flexible cantilever that deflects as a result of the force on the tip (Fig. 1a–c). The deflection of the cantilever is a quantitative measure of the force. To detect the deflection, a laser beam is reflected from the end of the cantilever into a detector. Through scanning, the interaction or the force between the tip and the surface is measured in a continuous feedback loop. The feedback serves to keep some of the parameters constant, allowing the measurement of the desired interactions.

AFM can be operated in four different primary modes that are distinguished by the way the tip is moved over the specimen. In the contact (static) mode [15], deflection is used as a feedback parameter by keeping the force constant. This mode is preferred especially for hard surfaces and single molecules, as the risk of damage is high for biological samples. In the non-contact mode [16], the cantilever oscillates at a small distance (1–10 nm) above the surface during the scan, without touching it. By keeping a constant distance, the changes in the amplitude, the frequency or the phase of the

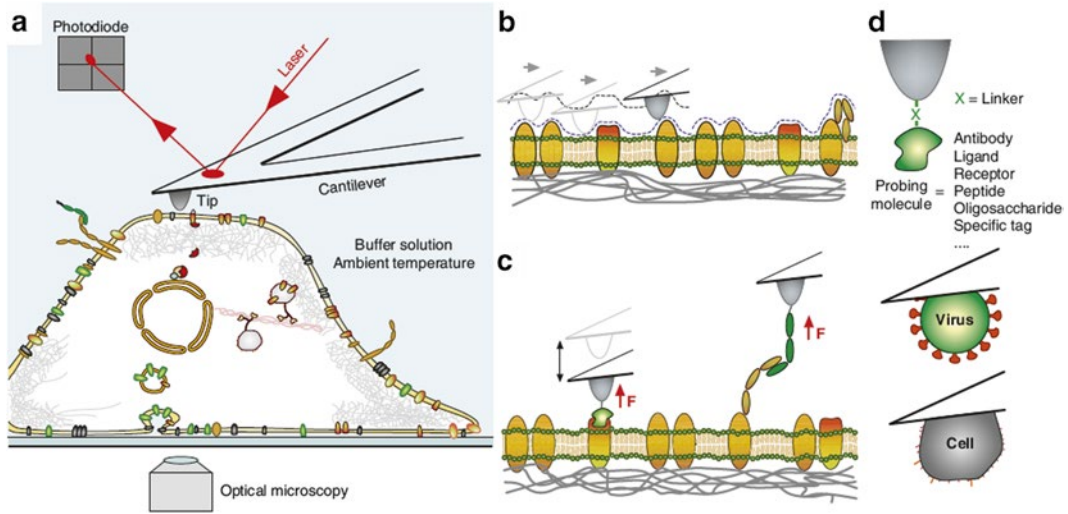


Fig. 1 Atomic force microscopy, for structural and functional imaging. **(a)** Use of AFM to probe the surface of a cell, in combination with modern optical microscopy techniques. **(b)** In the imaging mode, AFM scans the cell surface with nanometer resolution. **(c)** In force spectroscopy, the small interaction force acting between the AFM tip and the cell surface is measured while the tip approaches the cell and is retracted from the cell. **(d)** Various modalities may be used depending on whether the tip is functionalized with biomolecules or viruses or by a full cell. Reprinted with permission from [14]

cantilever are detected and used for feedback control. Attractive forces acting between the tip and the sample are sensed and topographic images are constructed. Another mode is the tapping mode [17] in which the tip briefly contacts the surface and then lifts off alternately. In this mode, the cantilever oscillates at higher amplitudes than the non-contact mode, which is advantageous to prevent trapping of the tip in thin liquid layer on the surfaces. It is especially used to image larger areas, which might have greater topographical variations. For biological samples, the last two modes are preferred, as the damage to the sample is greatly reduced. The fourth primary mode is the torsional resonance mode, where the cantilever oscillates in a twisting motion around its long axis. The twisting motion is changed upon the lateral forces the tip encounters and these changes are sensed by the detector [18]. There are also secondary imaging modes that are derived from the primary modes for detection of a specific type of interaction, such as friction forces between the probe tip and sample surface, conductivity or elasticity of the surface, electrostatic surface potential, temperature, magnetic force, or electric field gradients.

The biggest advantage of AFM is the possibility to attain single protein resolution in aqueous solutions. The resolution is in theory limited only by the apical probe geometry and the sample geometry (tip-sample dilation), but is also affected by the thermal noise and the softness of the sample. For example, for soft and dynamic cell

surfaces, such as those of mammalian cells, the typical resolution is 50–100 nm [14]. Although AFM offers high resolution and the possibility to probe various interactions, it has its own limitations. Since it is a surface scanning technique, only the top surface of the sample can be imaged at high resolution and the sample has to be immobilized on a support. For accurate results, effective vibration isolation is necessary. For biological samples, there is also the inherent risk of sample deformation by the tip. Live imaging is possible, but is typically rather slow (1 image/min). There are attempts to tackle this challenge by advancing the instrumentation, like incorporating high-speed scanners. Despite these disadvantages, AFM is a valuable tool for nanoscale resolution especially for in vitro characterization of biomolecules and has been employed for several biological questions. It has recently been used to observe the motion of single Kinesin-1 dimers along microtubules with enough resolution to observe both kinesin heads binding 8 nm apart to the same protofilament [19]. In another in vitro study, the mechanism of actin remodeling by a neuronal actin binding protein, drebrin A, has been investigated with subnanometer resolution [20]. Performing contact mode AFM imaging, nuclear pore complexes have been visualized together with ribonucleoprotein particles traversing the nuclear envelope [21]. AFM has also been used to study the conformation of various amyloid molecules in reconstituted membranes. The tested amyloid peptides (including α -synuclein, A β (1–40), amylin, and more) were found to form morphologically compatible ion-channel-like structures and elicit single ion-channel currents in reconstituted membranes [22].

The AFM-tip can be biologically modified to image-specific molecules in an approach called molecular recognition mapping (MRM [23]). For this purpose, various chemical groups can be adsorbed or immobilized on the tip (Fig. 1d). Molecules of interest, such as receptors, antibodies, ligands, tags, or even whole cells, can be conjugated to the chemically modified tip, usually through a linker molecule. By using modified tips, specific interactions can be probed [24] and interaction maps can be produced. This approach, for example, has been used to study the organization and rigidity of protein domains containing GPI-anchored proteins on neuronal membranes [25].

Apart from its use for imaging, AFM is also an important tool for force spectroscopic measurements and nano-manipulations. For example, the AFM tip could be employed to seize a single protein. By retracting the cantilever, the protein could be forced to unfold bond by bond and the amount of retraction could be measured to calculate the relative strengths of the chemical bonds [26, 27].

1.3 Total Internal Reflection Microscopy

When light encounters the interface between two media of different refractive indices, it bends (refraction). The refraction angle is determined by the refractive indices of the two media and the

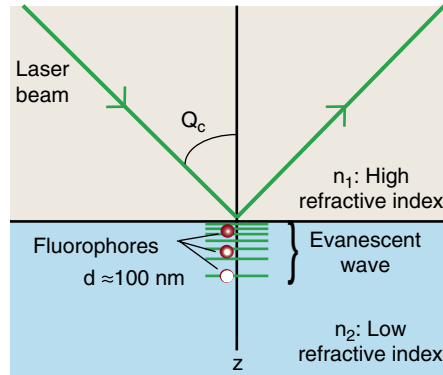


Fig. 2 The principle of TIRF microscopy. When a light beam arrives at an interface between media of different refractive indices (such as from glass into water), at an angle higher than the critical angle, it goes under total internal reflection. This generates an evanescent electromagnetic field at the other side of the interface at an intensity that decreases exponentially with the distance in z . TIRF makes use of this principle for excitation of only a subset of molecules that are very close (typically ≤ 100 nm) to the interface

incidence angle of the light. Refraction is usually accompanied by a small amount of reflection from the interface between the two media. If the light reaches the interface at an angle high enough, termed the critical angle, it refracts parallel to the interface. As the incidence angle increases toward the critical angle, the proportion of the refraction decreases and more light is reflected. When the angle is higher than the critical angle, the light coming through the first medium (of higher refractive index, such as glass) does not propagate in the second medium (of lower refractive index, such as an aqueous solution) and is instead completely reflected back from the interface (total internal reflection). In such a case, although the light itself stays in the first medium, an electromagnetic field, called “evanescent field,” is created in the second medium at close proximity of the interface. The evanescent field can only extend a few hundred nanometers in the z -direction, since the intensity decreases exponentially with the distance from the interface. TIRF microscopy (also called evanescent wave microscopy) exploits this principle to excite fluorophores that are in close vicinity of the specimen-glass interface [28]. The excitable region is typically restricted to a depth of less than 100 nm. To use the total internal reflection effect, TIRF setups provide laser excitation at an angle greater than the critical angle (Fig. 2).

As the physical principle suggests, the main characteristic of TIRF is restricting the fluorescence emission only to a very shallow region (≤ 100 nm) close to the coverslip. This greatly reduces the background and provides a high signal-to-noise ratio. Although the lateral resolution is not altered, it is possible to achieve high

axial resolution (typically ≤ 100 nm, but can be decreased down to 10 nm) on large fields of view without scanning. Thanks to the immense reduction in the background, high sensitivity, and minimized photobleaching, it is also a popular technique for single particle tracking approaches in the near-field [29]. TIRF is easily applied to live cell imaging and has been commonly employed for studies of dynamics near the surface. For instance, the inward movement of single clathrin-coated pits accompanied by dynamin recruitment and actin assembly has been visualized using TIRF [30].

Improvements in the TIRF methodology have also been important for advancement of other super-resolution techniques that rely on single molecule detection. By making use of the TIRF technique, it is possible to collect photons from single emitters, as the detection area is highly restricted. Provided that a sufficient number of photons are collected from single molecules, it is possible to find the localization of each molecule with very high precision by determining the centers of their PSFs. Thus, sub-diffraction localization information can be obtained from a diffraction-limited imaging process. The first of these TIRF-based single-molecule localization methods is “fluorescence imaging with one-nanometer accuracy” (FIONA [31]). Among its applications is the achievement of 10 nm axial resolution in living cells using TIRF and single-molecule localization for visualization of clathrin and its adaptor AP-2 in clathrin-coated pits [32]. The motion of secretory granules and the variations in their plasma membrane attachment have been visualized by TIRF as well, with detection of very small (<20 nm) axial displacements [33].

Although FIONA and its derivatives provide localization information with very high accuracy, they can only be used when the fluorophores are distant enough from each other. This is an important limitation for the wide-range biological applicability of these techniques. In this regard, one step forward was taken by incorporation of photoswitching or photoconversion of fluorophores, so that it is possible to detect individual fluorophores even when multiple emitters overlap. Super-resolution techniques that use this principle are explained below in more detail.

2 Far-Field Techniques

Despite the impressive resolution attainable by near-field techniques, the imaging power is limited to only a very thin section at (or close to) the specimen surface. Unfortunately, most cellular processes take place deeper in the cells. Far-field microscopy techniques enable detection at much larger distances than the wavelength of light, making them more easily applicable to biological questions.

2.1 Confocal Laser Scanning Microscopy

The confocal microscope has been invented and patented by Marvin Minsky in 1957 [34]. Although the main principles of his original design are still valid, several technological advancements have been incorporated into it over the decades. A modern confocal system consists of lasers for point-like and strong illumination of specimen, an illumination pinhole and an objective lens for obtaining a point-like focused scanning laser beam (point-like focal spot) and a detection pinhole for formation of a point-like image on a sensitive electronic photon detector. In this system, the point of focus on the object and the image are optically aligned to each other (conjugated together) along the path of light, hence the origin of the name “confocal” (having the same focus).

The main achievement of confocal microscopy is the elimination of the stray light and out-of-focus blur as the pinhole blocks the light emitted from the areas outside the focus. This gives clearer images and higher contrast, as well as the possibility to create optical sections. In a confocal microscope the contrast cut-off distance (the distance at which the contrast becomes zero and the intensity peaks cannot be distinguished) is smaller than for wide-field [35]. At the level of PSF, the higher contrast of the confocal microscope originates from a decrease in the height of the first diffraction ring in comparison to the central disk. It is especially useful for better separation of dim objects that are further away than the diffraction limit [36].

Theoretically, it is possible to achieve resolution beyond the diffraction limit in fluorescence imaging, by decreasing the pinhole size significantly lower than the Airy disk size. The attainable lateral and axial resolution improvement lies in the range of $\sqrt{2}$ fold [36, 37]. However, this is not very practical for the imaging of most biological specimens, as it causes a substantial decrease in signal-to-noise ratio due to the massive rejection of the emission signal by the small pinhole. Therefore, the lateral resolution improvement obtained with a confocal laser scanning microscopy (CLSM) is usually little or none, although the gain in contrast gives rise to crisper images. Nevertheless, the concept of the scanning confocal microscope has been used as a starting point for many high-resolution techniques.

2.2 Super-Resolution Microscopy Techniques

The techniques employed to attain high-resolution in the far-field differ in principle of operation, instrumental design, sample requirement and imaging capabilities. It is possible to classify them based on different aspects. Here, a basic classification is made according the main resolution-improvement strategies.

One general method to attain sub-diffraction resolution is to engineer/modulate the PSF. Techniques such as stimulated emission depletion (STED) microscopy [38] and structured illumination microscopy (SIM [39, 40]) modulate the geometry of the excitation beam by using non-linear optical effects and high-intensity lasers.

Another general method exploits the photoswitching/photoconversion properties of the fluorescent probes and spot localization at high-precision in the absence of nearby diffracting spots. This method led to a set of super-resolution techniques known as single-molecule localization methods, including stochastic optical reconstruction microscopy (STORM), photoactivation localization microscopy (PALM), fluorescence photoactivation localization microscopy (FPALM) [41–43].

A third strategy is to reconfigure the conventional objective geometry and light collection. The resolution improvement is achieved by increasing the fraction of the wavefront collected by the objective. 4Pi microscopy [44] and I⁵M [45] are the techniques that successfully apply this method to reach impressive levels of resolution especially in the axial dimension. In many cases, newer techniques arise by a modification or combination of these three concepts.

2.2.1 4Pi Microscopy

Most of the current super-resolution techniques (as explained below) give a higher priority to enhancing the lateral resolution. In contrast, 4Pi microscopy aims to increase the axial resolution, which is conventionally much lower than the lateral counterpart. For a single lens, the angle at which the spherical wavefront is collected is theoretically limited to 2π (where a full sphere encompasses an angle of 4π). However, in reality this requires a 90° semi-aperture angle, which is not attainable. By using two opposing lenses, this angle approaches the limit of 4π (hence the name 4Pi). If a spherical focal plane can be employed to collect the spherical wavefront, the image would not be as stretched as obtained with a planar focus plane [44]. 4Pi microscopy increases the aperture angle by placing two objectives opposite to each other, so that they have a common focus and the spherical segments of the wavefront can be collected from both sides, and interfered constructively. This gives rise to a 3–7-fold narrower main peak in the axial direction of the PSF. Thus axial resolution can be increased to 80–160 nm [46]. The lateral resolution however, stays the same (although crisper image details could be obtained, as the optical sections are thinner than in a conventional confocal microscope). Lateral imaging is performed through scanning. The specimen is generally placed in between two coverslips to maintain optical accessibility from both sides.

4Pi setups can differ in design depending on which beams are interfered [44]. Type A microscopes exploits only the interference of the excitation light and the emerging fluorescence is collected by a single lens; whereas Type B use only the interference of the emission light for coherent detection of the fluorescence. A third variant, Type C (Fig. 3a, b) combines A and B using two lenses both for excitation and emission [49].

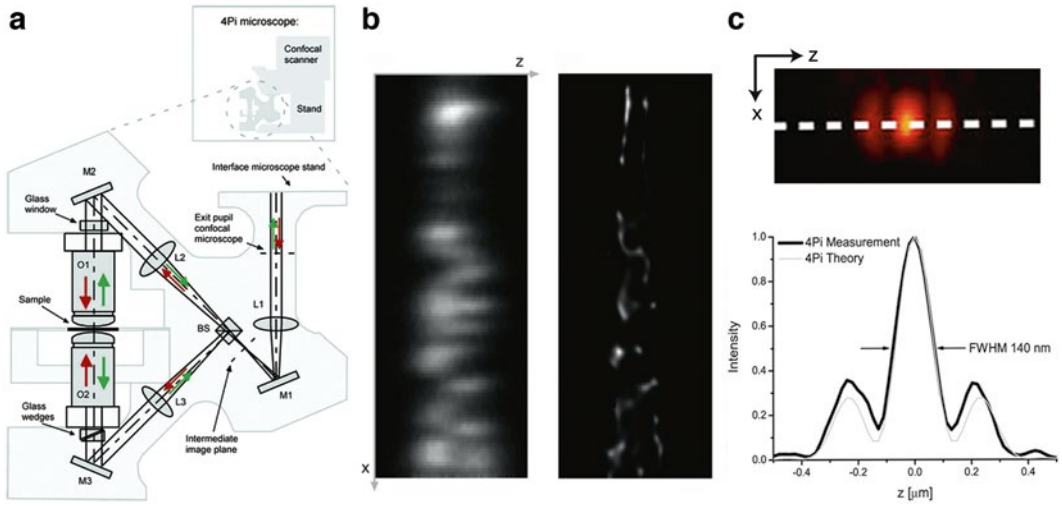


Fig. 3 4Pi microscopy. **(a)** Sketch of a 4Pi microscope (type C). Excitation light coming from the microscope stand is divided into two by the beam splitter (BS) and both beams are focused onto the same sample spot by the opposing objective lenses O1 and O2. The intermediate optical system consisting of the lenses (L1, L2, and L3) and the mirrors (M1, M2, and M3) maintain the beam paths for point scanning with two objective lenses. Fluorescence collected by both lenses meet at BS, and led back to the microscope stand. The movable glass wedges and the glass window are used to adapt the system for dispersion of light at a range of wavelengths. A standard confocal microscope unit is used for scanning. Reprinted with permission from [46]. **(b)** Confocal (*left*) and restored 4Pi-confocal (*right*) XZ-images of microtubules in a cell. The 4Pi image has an axial resolution in the 100-nm range. Scale bar is 400 nm. Reprinted with permission from [47]. **(c)** XZ-image of a 100 nm fluorescent bead taken by a type A 4Pi-confocal microscope. The line profile along the dashed white line displays side lobes of 35 %, which can be removed through deconvolution. The measured FWHM is very close to the theoretical value. Reprinted with permission from [48]

Interference of the two equal wavefronts of opposite directions generates a standing wave that does not propagate and stays in a constant position. This kind of wave results in the formation of two smaller secondary maxima next to the main PSF peak (more explicitly below and above according to the specimen plane). These secondary interference maxima are called “side lobes” and can cause ghost images if not removed properly (Fig. 3c). To remove the side lobes, a deconvolution procedure has to be applied (deconvolution is the mathematical reversion of the optical distortion that takes place in a microscope, in order to improve the image quality). The higher these side lobes are, the harder it gets to remove them by deconvolution. As a general rule, if they are higher than 50 % of the main PSF peak, it is not possible to get unambiguous data [48]. The height of the side lobes decreases with increasing semi-aperture angle. With most available immersion lenses the semi-aperture angle would be below 68° , giving primary side lobes higher than 60 % of the main peak [50]. Therefore, in order to suppress the side lobes, other optical modifications are generally

used, including addition of a confocal pinhole to decrease the fluorescence detection from the side lobes or using two-photon excitation [51], which decreases the height of side lobes relative to the main peak. Two-photon excitation also enhances the effect of the confocal pinhole, as longer excitation wavelengths move the side lobes away from the focal plane [44]. In general Type C setups are better at lowering the side lobes. The best results are therefore obtained by using a confocal Type C 4Pi microscope with two-photon excitation [46, 49].

4Pi microscopy has been used for mammalian cells to visualize in dual-color the Golgi stacks [48] and nuclear pore complex components [52] with 110–130 nm axial resolution. For live imaging, there are a few compromises. First, the specimen needs to be mounted in aqueous medium, which creates a refractive index mismatch between the mounting and the immersion medium used for high numerical aperture oil-immersion lenses. This mismatch deforms the spherical detection of the wavefronts and causes higher side lobes. Water-immersion lenses need to be used to prevent the mismatch. However, these lenses have smaller aperture angles compared to oil-immersion lenses, consequently enhancing the side lobes [53]. To account for that, it is necessary to apply multi-photon excitation. Second, as in some other super-resolution techniques, the focal volume is reduced to improve the resolution. This gives rise to a reduction in total fluorescence and a decrease in signal-to-noise ratio. Therefore, the recording time should typically be increased to reduce the noise, in order to compensate for the decreased volume. To counterweigh this problem 4Pi setups with parallelized recording from multiple foci have been designed. This design is called “multifocal multi-photon microscope” (MMM-4Pi [54, 55]). This modification, together with confocal pinholes and image restoration, has been useful to obtain 3D images of the mitochondrial network in living yeast at an equilateral resolution of ~100 nm [56]. Live mammalian cells have also been imaged with a similar 3D resolution, using a GFP-labeled Golgi marker [57].

In addition to imaging at high resolution, the shape of the 4Pi PSF has offered a new tool to quantify the thickness of cellular structures (varying between 75 and 500 nm) with high precision. For this quantification the ratio of the average value of the two primary minima to the average value of the two side maxima is calculated. The smaller the ratio (the higher the side lobes relative to the primary minima), the thinner is the object [53]. This measurement was used to quantify the average diameter of the tubules of the mitochondrial network [56].

In order to reach super-resolution in 3D, 4Pi has also been employed in combination with super-resolution techniques of high lateral performance such as STED microscopy [58], as will be detailed below.

2.2.2 I^5M

I^5M is technically related to 4Pi. It is a combination of two kinds of interference-based approaches, image interference microscopy (I^2M) and incoherent interference illumination (I^3) [59]. I^2 and I^3M can be said to be wide-field counterparts of type B and type A confocal 4Pi microscopy, respectively. In the I^2M mode, emission beams are collected from two opposing objective lenses and after traveling over different paths with equal distances they are superimposed on one CCD camera. The image is formed through interference of the two fluorescent beams. In the I^3 mode, the sample is illuminated from both sides using an incoherent light source such as a standard arc lamp, in contrast to a laser as in 4Pi. The illumination light is polarized perpendicular to the axial direction, so light beams coming from opposite directions interfere at the focal plane creating standing waves [53] that excite a narrower area. Emitted fluorescence is detected by a CCD camera. By combining I^2M and I^3 , I^5M attains high axial resolution through interference in both excitation and emission detection, in a similar fashion to type C confocal 4Pi microscopy, but operating in the wide-field context with single-photon illumination [60].

The FWHM of the I^5M PSF is typically comparable to that obtained by 4Pi, ~ 7 times narrower than conventional wide-field microscopy. However, compared to 4Pi, the side lobes are more pronounced in I^5M . On the other hand, I^5M is faster and has a lower-cost, and can obtain more photons as single-photon excitation is used. Still, the difficulty of removing comparatively higher side lobes has been limiting widespread biological applications of I^5M .

The compromises for live 4Pi imaging are also valid for I^5M ; however, the generally elevated side lobes in I^5M cannot be as easily compensated. Therefore, so far significant resolution improvement by I^5M has only been demonstrated with oil immersion lenses, limiting its use to fixed samples [53]. Under favorable conditions, better than 100 nm axial resolution has been experimentally verified imaging filamentous actin in fixed mammalian cells [45].

Like 4Pi, for 3D resolution improvement, I^5M has also been combined with other super-resolution techniques, for example, SIM (I^5S [61]), giving rise to ~ 100 nm resolution in all dimensions.

2.2.3 *Stimulated Emission Depletion Microscopy*

STED microscopy exploits the physical phenomenon known as “stimulated emission” to modulate the effective PSF. If an electron in excited state encounters a photon at an energy level similar to the difference between the electron’s energy and the ground energy, the photon will stimulate the electron to fall into the ground energy state. This is realized through emission of a photon with the same wavelength as the incoming one. The excited molecule is therefore not allowed to undergo spontaneous emission of a fluorescence photon, but is subject to STED and will emit a photon at the wavelength of the light used for the STED effect. These more red-shifted photons can be separated from the

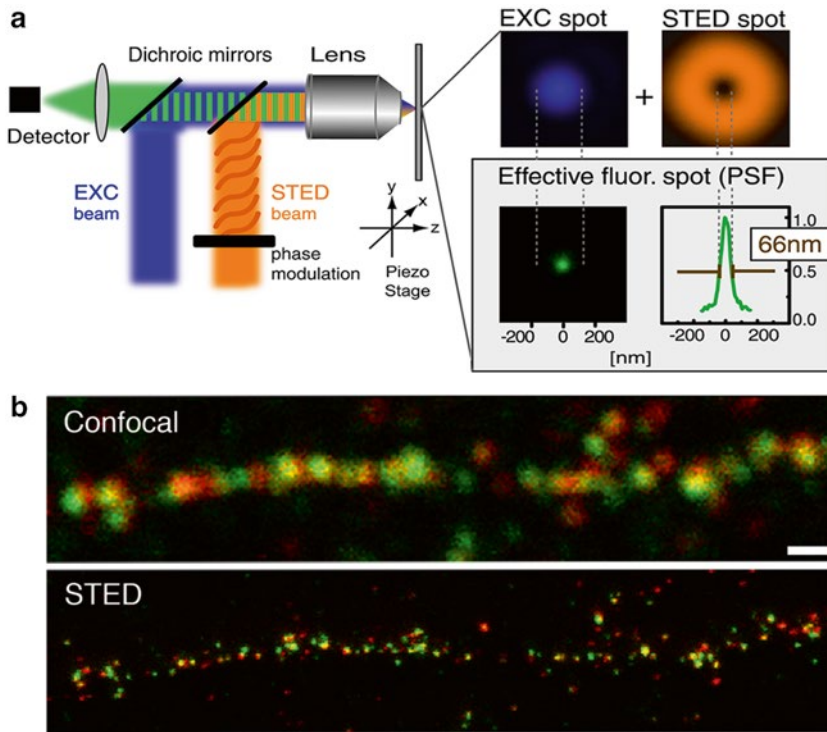


Fig. 4 STED microscopy. **(a)** Principle of operation. The excitation beam (*blue*) is superimposed with a doughnut-shaped depletion beam (*orange*), resulting in the de-excitation of all fluorophores except those located in the center of the depletion beam. This yields an effective fluorescent spot of sub-diffraction size (*green, below*). Reprinted with permission from [63]. **(b)** Synaptotagmin 1 (*red*) and synaptophysin (*green*) colocalize well on the plasma membrane of neurons, after vesicular fusion, as visualized by STED microscopy. Note the precision of the full or partial colocalizations in the two-color STED image over the confocal counterpart. Scale bar is 1 μm . Reprinted with permission from [64]

fluorescence emission by use of filters. Fluorescent dyes can thus be “de-excited” by additional irradiation with a red-shifted depletion beam: STED. The STED microscope functions like an improved confocal laser-scanning microscope, in which a conventional excitation beam is used to turn on the fluorophores in a diffraction-limited spot. The additional feature is the introduction of a second (STED) beam that is modulated by a phase plate into a doughnut-like shape. By alignment of the two beams, the emission of fluorescence is only allowed from the center of the excited spot where the depletion beam has zero intensity, so a much smaller focal spot can be obtained [38, 62], resulting in images with substantially higher resolution (Fig. 4). The image is generated through scanning of the chosen area. The obtained improvement in resolution is theoretically not limited by a physical barrier. In principle if the intensity of the de-excitation beam is high enough, the focal spot can be decreased to molecular size [65].

Since STED was the first of the many following diffraction-limit breaking strategies, and has been used to address biological questions for over a decade, it is worthwhile to go briefly through the key studies that contributed to the development of the technique. The development timeline of STED microscopy, as detailed below, is a good example of the typical steps by which a super-resolution technique emerges in biology. New techniques are put forward first by demonstration of the use of an optical/physical phenomenon to obtain high-resolution with a proof-of-principle study, followed by application to a simple, fixed biological specimen such as bacteria. Then, the advantages of the technique are demonstrated on more complex samples, to answer previously unresolvable biological questions. Next, the technique is adapted to the needs of biology by making implementations enabling multicolor imaging, reduced sample damage, live imaging, high temporal resolution, broader fluorophore selection, further-improved or 3D super-resolution, as well as easier operation and lower costs. In the course of development, the commercialization of the specialized equipment is also important for the new technique to become widely used.

The theoretical principles of STED microscopy were first introduced in 1994 by Hell and Wichmann [38]. Later in a proof-of-principle study the proposed setup, which featured an axially modulated PSF, was used on living yeast and *E. coli* cells [62]. A fluorescent spot of 18-times smaller focal volume was obtained. This was followed by implementation of STED in a 4Pi fashion, giving rise to an axial resolution of 33 nm. The focal spot size of $\lambda/23$ was the lowest obtained in far-field microscopy by 2002 [66]. Until this point, solely membrane dyes were used for labeling. Since the resolution is highly dependent on the high excitation intensity it was questionable if similar sub-diffraction resolution could be obtained with other types of labeling. Therefore the next important study applied STED to a conventional immunofluorescence preparation and microtubules of mammalian cells were imaged at an axial resolution of ~50 nm, with a 4Pi-STED setup. The resolution improvement obtained with STED was until this time point largely axial (along the optical axis) due to radial polarization of the STED beam and was also accompanied with higher side lobes, which required extra image processing. In a 2005 study, the phase plate that modulates the STED beam was modified into a doughnut-shaped composite to obtain sub-diffraction resolution in the focal plane, yielding a lateral resolution of 16 nm [67]. With this version of the setup it was experimentally proven that the resolving power increases with the square root of the saturation level of STED. Therefore, for

calculation of resolution in such microscopes the Abbe equation [68] is replaced with the following:

$$\Delta r \approx \frac{\lambda}{2 \sin \alpha \sqrt{1 + \frac{I}{I_{\text{sat}}}}} \quad (1)$$

where λ and α denote the wavelength and aperture angle of the lens, respectively. I is the maximal focal intensity applied for STED and I_{sat} is a characteristic value at which the fluorescence excitation is reduced to half [63, 67]. Here it could be seen that when I/I_{sat} is increased toward infinity, resolution (Δr) approximates to zero; hence resolution is now independent of diffraction.

After this point, STED was applied to biological questions. One of the best-known applications was performed to answer a neuroscience question: do the components of synaptic vesicles diffuse on the plasma membrane or do they remain together after exocytosis? Synaptic vesicles are ~40 nm in diameter and are densely packed with proteins making them or their constituents very hard to resolve. Using STED, it was possible to show that the vesicle membrane protein Synaptotagmin 1 is found in patches of 70 nm on the plasma membrane after fusion of the vesicle [63]. In another study STED was used to visualize the active zone protein Bruchpilot in *Drosophila* synapses and neuromuscular junctions. Surprisingly, the protein was found to form ring-shaped structures, which could not be resolved with confocal microscopy [69].

In 2006, fluorescent proteins (following membrane dyes and organic-dye conjugated antibodies) were shown to be compatible with STED [70]. These studies continued with introduction of two-color STED, which enabled simultaneous super-resolution imaging in multiple colors. For that it was necessary to use two pulsed laser diodes for excitation at different wavelengths and two amplifiers for two STED beams of different wavelengths. A lateral resolution of 30 and 65 nm was obtained for fluorescent beads imaged in the green and the red color channels, respectively [71]. 3D imaging with the STED technique was also made possible by introduction of isoSTED [58]. This setup used two different STED beams of the same wavelength orthogonal to each other so that the STED effect is obtained both laterally and axially. It also had a 4Pi-like organization, using two opposing lenses to collect more of the wavefront. As a result, a spherical focal spot was obtained with ~40 nm resolution in each dimension. By making optical stacks, high-resolution 3D images of mitochondria (immunolabeled against Tom20) were obtained. The method was also used with the addition of a second color, displaying a homogeneously distributed mitochondrial matrix protein together with the outer membrane protein Tom20, which was found to form distinct clusters at the organelle's boundary. In parallel, a more

economical and easy-to-use laser source, continuous wavelength (CW) laser, was used instead of the more expensive and complicated pulsed-laser [72]. This development increased the accessibility of the technique for more laboratories, as well as the speed of image acquisition.

STED was also applied to live, deep tissue imaging. Neurons were filled with YFP and the morphological changes of dendritic spines (with structures ≤ 40 nm) were imaged in time-lapse after stimulation [73]. The fact that the technique requires scanning makes it relatively slow. However, when small fields of view are taken, it is possible to make video-rate (28 frames per second) movies with a fast scanner and a fluorescent label with high photon yield. This was demonstrated by imaging synaptic vesicles in living neuronal preparations. It was possible to track these small organelles and identify different pools based on their speed [74, 75]. Another biologically useful effort was combining advantages of STED and electron microscopy in a correlative fashion to obtain specific protein localization information in the morphological context of the cell [76]. Of course, this kind of correlation microscopy requires the fixation and embedding conditions to be optimized to get the best of both techniques. Finally, STED was shown to be applicable to multicellular living organisms. Fluorescent proteins were expressed in neuronal cells of *C. elegans* and in the brain of an adult mouse [77, 78]. In both cases, axonal or dendritic structures in neurons were imaged with 110 and 67 nm resolution, respectively, for *C. elegans* and mouse brain.

As could be seen from all these applications, STED microscopy has undergone various modifications to satisfy the needs of biology. Every adaptation though, as one would expect, has the risk of complicating the instrumentation. Also economically, a STED setup is rather costly. Still, its key advantage is the fact that it does not require image processing and the super-resolution image is obtained right during acquisition. Fifty to 70 nm resolution is commonly reached, while it is possible to reach much higher resolution under optimized conditions. The fluorophore choice depends on the capabilities of the setup used, and is still limited to bright and rather photostable fluorophores whose spectral properties match that of the available lasers for a particular setup.

2.2.4 Structured Illumination Microscopy

SIM is a wide-field (non-scanning) technique. It is sometimes also called “poor man’s confocal microscope,” referring to its immense optical sectioning ability without the use of an expensive confocal system [79]. In a conventional SIM configuration, a periodic diffraction grating of known pattern is inserted in the illumination beam path and is projected onto the sample [39]. This causes the formation of interference patterns (referred to as “moiré fringes”) in the emission (Fig. 5a). Moiré patterns are generated by multiplication of the initial pattern (of known periodicity) with the

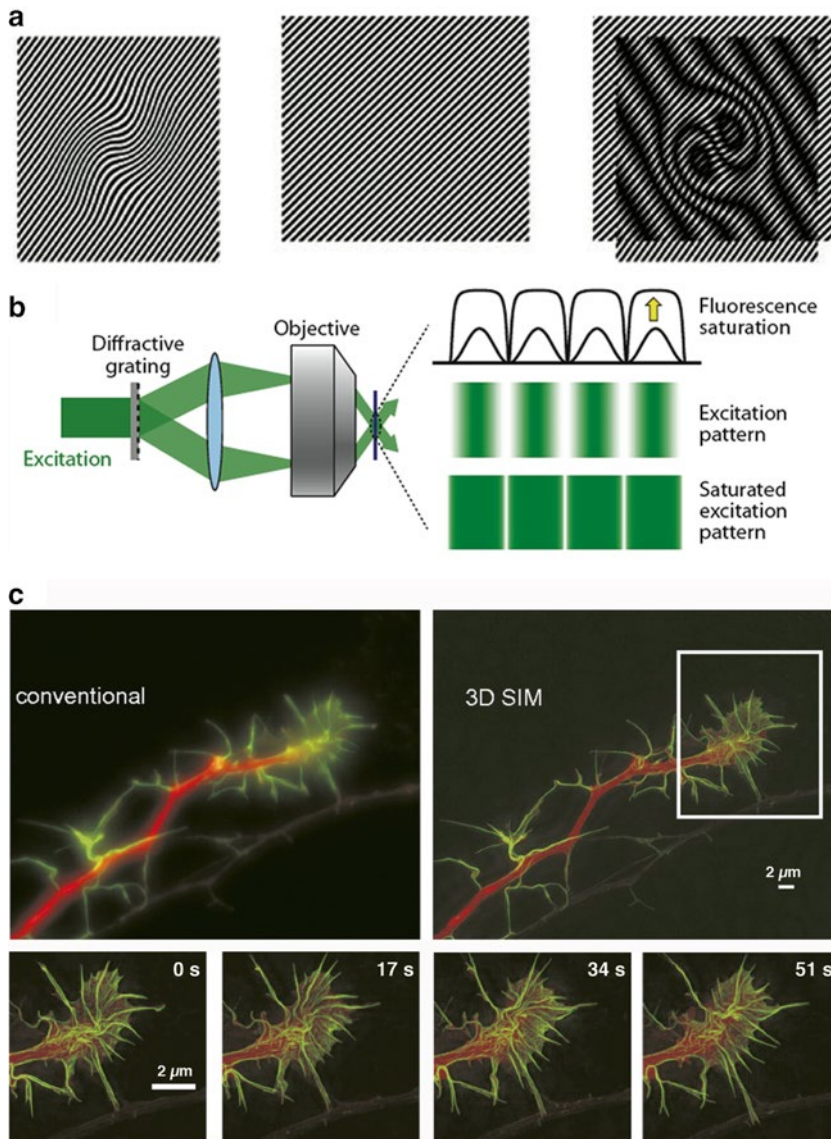


Fig. 5 Structured illumination microscopy. (a) Resolution extension through the moiré effect. When a known regular illumination pattern is applied to a sample, moiré fringes are generated at a significantly lower spatial frequency than that of the sample and imaged by the microscope. Multiple images that resulted from scanning and rotating the excitation pattern are then used to reconstruct the sample structure. Reprinted with permission from [40]. (b) The principle of SIM and SSIM. A diffractive grating placed in the excitation path causes the single light beam to split. The interference of these after passing the objective creates a pattern with alternating peaks and zero points. For SSIM, the strong excitation light creates sharper transitions, as it saturates the fluorescence emission at the peaks, while not changing the zero points. Reprinted with permission from [80]. (c) Live two-color 3D SIM imaging of cultured hippocampal neurons. To reveal the actin structure in the growth cone, actin was labeled with tdTomato-LifeAct (pseudocolored in *green*) and cytosol was labeled with GFP (shown in *red*). Live images were collected for 20 time points, with each time point acquired within 17 s. *Top panel* shows the maximum intensity projections (along the z-axis through the entire 3 μm volume thickness) for the conventional and SIM images for the first time point. Magnified images of the boxed region at different time points are shown in the *bottom panels*. Reprinted with permission from [81]

unknown sample periodicity. The resulting interference pattern can be used to back-calculate the spatial information from the sample. For that, it is necessary to collect a number of images by applying the illumination pattern in different orientations (a minimum of 3 per position). Because the moiré fringes are much coarser than both the original illumination pattern and the sample information, they are easily detected and can be used to gain spatial information that is normally unresolvable. In the case of patterned illumination, Abbe's limit for detection is extended by addition of the spatial frequencies in the pattern. Therefore, the resolution improvement is proportional to the spatial frequency of the illumination pattern. Here, the maximum spatial frequency is obtained by summing the highest spatial frequency in the patterned illumination and highest frequency detected [82]. Since the pattern itself is also diffraction limited, the lateral resolution increase by this summation is maximum twofold [83].

Nevertheless, by using optical nonlinearity near saturation the resolution could be further improved [84]. This is achieved by saturated structured illumination microscopy (SSIM [40]). When illumination is strong enough to excite most of the fluorophore molecules, additional increases in the illumination intensity will not give a linear increase in emission intensity (Fig. 5b). The non-linearity is achieved near or above the saturation threshold for excitation. Using saturated illumination, a non-linear relationship between excitation and emission is obtained. This allows generation of moiré fringes with higher spatial frequencies than the initially applied illumination pattern and in turn results in a higher resolution [40].

SSIM theoretically offers unlimited resolution, as the resolution depends on the level of saturation [40]. However, in practice photobleaching of the dyes and decreasing signal-to-noise ratios are the limiting factors. For beads, resolution below 50 nm has been achieved [40]. An alternative to saturation (that employs high-laser power) is to use photoswitchable probes. Photoswitchable molecules can be reversibly switched between two different emission states by exposure to light of low intensities. Exploiting the photoswitching phenomenon, a non-linearity is created by saturation of the population of fluorophores in one or the other state. In an exemplar study, a photoswitchable protein, Dronpa, was used to get ~55 nm resolution in mammalian cells applying non-linear SIM with modest levels of excitation [85].

It is also possible to obtain high-resolution both in the lateral and axial direction using 3D SIM [86]. For example, multi-color 3D SIM has been applied to study the mammalian nucleus at 100 nm resolution in 3D and it was possible to resolve the chromatin, nuclear lamina and single nuclear pore complexes along the nuclear periphery [87]. Multicolor 3D SIM was also applied for live imaging of neurons (Fig. 5c) to visualize the complex actin structure in the neuronal growth cone [81]. Another 3D

implementation, I⁵S [61], combines SIM with I⁵M to obtain ~100 nm resolution in three dimensions.

The most important advantage of SIM or SSIM is the ease of performing multi-color imaging (three or more) with any bright and photostable fluorophore. 3D high-resolution imaging is possible (although for SSIM this increases the photobleaching problem). Live imaging is generally restricted to slow-moving structures, because ideally the specimen should not move during the rotation of the grating. However, with the development of faster cameras or use of multifocal setups, it is possible to perform faster image acquisition for live imaging [81, 88]. In general, it is necessary to take ~10 raw images for SIM and ~100 for SSIM to computationally reconstruct a super-resolution image and heavy post-processing is required [82].

2.2.5 Pointillistic Techniques: Super- Resolution Imaging Using Single-Molecule Localization

To obtain high resolution, it is not always necessary to use sub-diffraction images. If a sufficient number of photons are collected, the position of a single fluorophore can be calculated with nanometer precision [89]. The issue is to evade the crowding that prevents getting signal from single emitters. In 2006, three different studies reported a new type of super-resolution microscopy strategy. Although the techniques were named differently as photoactivated localization microscopy (PALM [42]), STORM [41] and fluorescence photoactivation localization microscopy (FPALM [43]), they used essentially the same strategy: single-molecule switching to find the localization of single molecules with high precision. The strategy is based on photoactivation/photoswitching of fluorophores such that at one time point there would be only one fluorophore emitting per diffraction limited area, enabling calculation of the localization for each fluorophore. By repeating such imaging cycles many times to collect photons from all the fluorophores, an overall image can be reconstructed. Before imaging, the fluorophores are either in the default off-state (photoactivatable—PALM, FPALM) or a strong pulse is applied to switch them all off (photoswitchable—STORM). Then they are switched on/activated stochastically and imaged until they switch off or bleach. This is repeated until all the fluorophores are captured (Fig. 6a, b). The techniques based on this approach are collectively referred to as single-molecule localization microscopy or pointillistic microscopy [92].

The resolution, in this case, is independent of the wavelength and is dependent on the density and accuracy of the localization. In principle, the more photons detected from the molecule, the better is the localization precision. Essentially, the uncertainty in localization is inversely proportional to the square root of the number of photons detected [89, 93]. Approximately:

$$FWHM_{localization} \approx \frac{FWHM}{\sqrt{N}} \quad (2)$$

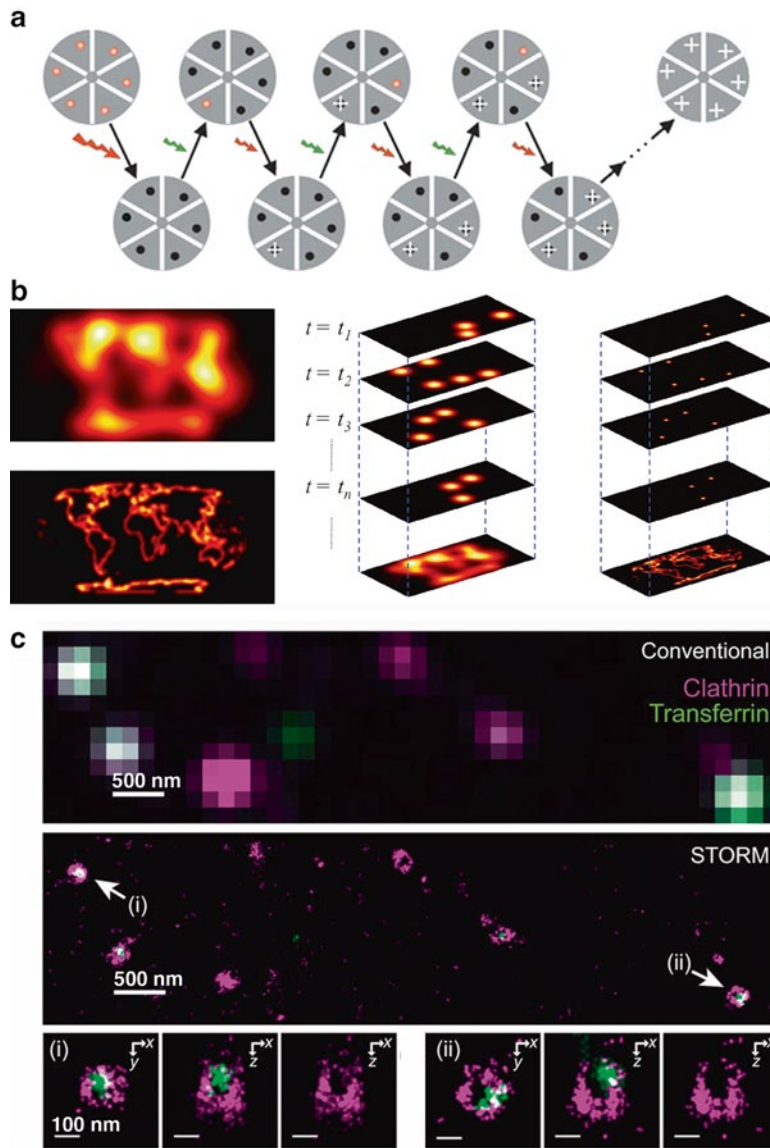


Fig. 6 Pointillistic imaging. **(a)** STORM with photo-switchable fluorophores. The scheme shows the imaging sequence for a hexameric object labeled with red fluorophores. The fluorophore can be switched between a fluorescent and a dark state by application of red and green laser, respectively. Initially, all fluorophores are switched off (the dark state) by a strong red laser pulse. Then, in each imaging cycle, a green laser pulse is applied to switch on just a fraction of the fluorophores so that an optically resolvable set of active fluorophores can be imaged. After being switched on, the emission is collected from the active fluorophores under red illumination. This allows their positions (*white crosses*) to be determined with high precision. The final image is generated by reconstruction of all the fluorophore positions collected through several imaging cycles. Reprinted with permission from [41]. **(b)** The principle of PALM. The sample is imaged by repeated cycles of activation, localization, and bleaching individual emitters to reconstruct a high-resolution picture. Reprinted with permission from [90]. **(c)** Live two-color 3D STORM with astigmatism-imaging of transferrin and clathrin-coated pits. SNAP-tagged clathrin was labeled with Alexa647 (*magenta*) and transferrin was directly labeled with Alexa568 (*green*). *Top panel* shows the conventional live image, and below is the *x-y* projection of the 3D STORM image (taken in 30 s). For the structures indicated by *arrows (i) and (ii)*, *x-y* cross-sections near the plasma membrane (*left*), *x-z* cross-sections cut through the middle of the invaginating coated pit (*middle*) and corresponding *x-z* cross-section of the clathrin channel (*right*) are displayed at higher magnification in the *bottom panels*. Reprinted with permission from [91]

where $\text{FWHM}_{\text{localization}}$ is the localization precision, FWHM is obtained from Gaussian fitting of the PSF of the emitter and N is the number of photons captured from a single fluorescent molecule and varies from fluorophore to fluorophore. If, for example, 10,000 photons could be gathered in the active state of the fluorophore, it would be possible to reach 1–2 nm accuracy. One problem is the background and the residual emission of the photoactivatable/switchable fluorophores. Therefore, an important criterion for the fluorophore choice is the contrast ratio, which is the ratio of the emission after photoswitching/activation to the emission in the dark state. For this reason, in parallel to the technical developments in the pointillism imaging, many fluorescent probes are actively being characterized for their applicability for pointillism.

Initially, STORM has been demonstrated using a cyanine switch, which consists of a Cy3-Cy5 dye pair. Cy5, a commonly used cyanine dye, can be switched to a stable dark state by the same red laser light that is used for excitation of the dye. Green laser light is then used to convert Cy5 back to its fluorescent state. To increase the recovery rate, a Cy3 dye is placed in close proximity to Cy5 [41]. The fluorescent probes designed this way consist of a reporter that can be photo-switched on and off, and an activator that is required for the efficient photoactivation of the reporter. Using this pair it was possible to gather ~3,000 photons per switching cycle, predicting a theoretical localization accuracy of 4 nm. The primary cyanine switch has also been generalized to enable multi-color imaging. Various paired switches can be combined for multi-color imaging. For example, three different activator molecules were paired with the same reporter, to visualize immobilized DNA molecules, microtubules and clathrin-coated pits in fixed mammalian cells with 25 nm resolution [94].

For PALM, photoswitchable/activatable variants of the fluorescent proteins, such as photoactivatable GFP (PAGFP [95]), have been the most commonly employed fluorophores. PALM has been used in probing protein clusters in the plasma membrane, by expressing PAGFP. For example, the nanoscale distribution and kinetics of influenza hemagglutinin clusters on fibroblast cell membranes were imaged at 40 nm resolution in living cells, using PAGFP [96]. In another study pointillism has been employed to uncover the clustered distribution of the chemotaxis receptors tagged with a different photoactivatable fluorescent protein, tandem-dimer Eos (tdEos), on the cell membrane of *E. coli* [97]. Using localization microscopy techniques, it is also possible to perform single-particle tracking with high spatial precision in living cells. For example, a highly spatially resolved maps of single-molecule motions have been created by imaging the membrane proteins Gag and VSVG, through labeling with EosFP [98].

Localization microscopy has also been modified for 3D high-resolution imaging. For instance, by insertion of a cylindrical lens in the imaging path, the information obtained from each

fluorophore image can be increased. The centroid still gives the lateral positioning, whereas the shape or the ellipticity becomes a measure of the distance from the focal plane [99]. As a result, using the astigmatism of the image, the axial position can be determined. By this additional functionality, clathrin-coated pits in fixed cells have been imaged with ~25 nm lateral and ~55 nm axial resolution [100]. 3D STORM with astigmatism was also applied in live, two-color fashion yielding <25 nm lateral and ~60 nm axial resolution [91]. This way it was possible to resolve the morphology of the clathrin coat enclosing the transferrin cargo (Fig. 6c). Recently, dual-objective astigmatism-based 3D STORM has revealed the surprising actin ultrastructure in fixed neurons [101].

3D PALM has also been demonstrated through interferometric photoactivated localization microscopy (iPALM), which uses a dual lens system as in I⁵M and collects the phase information through interference of photons coming from single fluorescent molecules and traveling different light paths. Employing iPALM, microtubules have been imaged with 25 nm 3D resolution [102].

Pointillistic approaches make the instrumentation relatively simple and can yield 10–40 nm resolution. Instead of scanning the sample, 100–100,000 frames are collected by a camera for one image. This means, on the other hand, that imaging is slower and post-processing is required as single emitters should be extracted from many frames and their localizations should be obtained computationally to reconstruct the final super-resolution image. Development of camera systems with single-photon sensitivity (electron multiplying charge-coupled devices, EMCCD) has been of great use for pointillistic methods, especially in terms of improving the time resolution.

The other requirement for pointillism is the necessity to use photoswitchable/activatable fluorophores. Theoretically, it is also possible to exploit the spontaneous blinking behavior of many fluorophores, including many of the Alexa and cyanine dyes. However, most of the time it is necessary to use oxygen-free redox buffers including reagents such as mercaptoethanol, glutathione or other oxygen scavengers to enhance blinking. Nevertheless, the repository for such fluorescent proteins and organic dyes is growing. Recently developed caged fluorophores (bearing a photocleavable cage moiety that can turn the fluorophore non-fluorescent) enable photoswitching without use of high concentrations of oxygen scavengers [103, 104].

3 A Comparison of the Super-Resolution Techniques

The super-resolution techniques presented above all come with specific advantages and disadvantages. It is hard to point out the best technique for super-resolution imaging, as the answer would be very much dependent on the particular application and the experimental requirements. Table 1 summarizes and compares the

Table 1
Comparison of far-field techniques

Technique	CLSM	STED	(S)SIM	PALM/STORM/FPALM
X, Y-resolution	Typical Best	200–250 nm – 40–80 nm 10 nm	100–130 nm 50 nm	20–50 nm 10 nm
Z-resolution	Typical Best	500–700 nm – 500–700 nm 20–100 nm	250–300 nm 100 nm	100 nm (TIRF implementation) 10–25 nm
Detection	Scanning	Scanning	Wide-field	Wide-field
Fluorophore choice	Broad	Restricted (dyes with appropriate STED characteristics)	Broad	Restricted (preferentially photoswitchable/activatable)
Live cell imaging	Yes	Restricted	Restricted	Restricted
Speed of imaging	Typical Best	Milliseconds to seconds Milliseconds	Seconds to minute Milliseconds	Seconds to minute Seconds
Multicolor imaging	Typical Best	1 2	1 ≥3	1–2 ≥3
Data processing requirement	No	No	Yes	Yes
Complexity of the hardware	Medium	High	Medium to high	Low to medium
Bleaching	Medium	High	Medium to high	Medium to high
3D implementation	4Pi	isoSTED	3D SIM I ⁵ S	3D STORM with cylindrical lenses iPALM

capabilities of the most commonly used far-field techniques. However, it should also be kept in mind that this table can change significantly over time, as these techniques are continuously being improved with new studies coming forward almost at a weekly basis. New results at the nanoscale also come with new challenges. The higher imaging precision gained by super-resolution is showing us not just prettier pictures, but also higher-complexity images that require a perspective change in terms of interpretation of new observations and re-thinking of the pre-existing ones [105, 106]. For example, “colocalization” experiments in super-resolution studies are presenting an improved precision and higher detail. Information obtained with some of the conventional imaging studies is becoming inadequate at the nanoscale, creating the necessity for more descriptive research at high-resolution. Previously unexpected observations, such as nanoscale domains of various kinds, are becoming apparent and new functional hypotheses have been pushed forward [106]. On the other hand, new schemes of data analysis and processing are being established to obtain more information from the newly arising and increasingly more complex data.

The improvements in imaging techniques also require methodological changes in sample preparation and labeling. As we reach higher resolution, the sizes of the fluorescent probes start to matter as much as their optical properties [107, 108]. Antibodies or fluorescent proteins are slowly becoming too big, and smaller probes and tags with minor target modifications are being developed.

Overall, with the new array of super-resolution microscopes and the methodologies developed in parallel, we are coming a bit closer to seeing and understanding the important cellular processes that have been waiting to be explored, just beneath our resolving power.

References

1. Synge EH (1928) XXXVIII. A suggested method for extending microscopic resolution into the ultra-microscopic region. *Philos Mag* 6:356–362
2. Ash EA, Nicholls G (1972) Super-resolution aperture scanning microscope. *Nature* 237:510–512
3. Lewis A, Isaacson M, Harootunian A, Muray A (1984) Development of a 500 Å spatial resolution light microscope. *Ultramicroscopy* 13:227–231. doi:[10.1016/0304-3991\(84\)90201-8](https://doi.org/10.1016/0304-3991(84)90201-8)
4. Pohl DW (1994) Near-field optics: light for the world of NANO. *J Vac Sci Technol B* 12:1441. doi:[10.1116/1.587313](https://doi.org/10.1116/1.587313)
5. Durig U, Pohl DW, Rohner F (1986) Near-field optical-scanning microscopy. *J Appl Phys* 59:3318. doi:[10.1063/1.336848](https://doi.org/10.1063/1.336848)
6. Betzig E, Trautman JK (1992) Near-field optics: microscopy, spectroscopy, and surface modification beyond the diffraction limit. *Science* 257:189–195. doi:[10.1126/science.257.5067.189](https://doi.org/10.1126/science.257.5067.189)
7. Gerton J, Wade L, Lessard G et al (2004) Tip-enhanced fluorescence microscopy at 10 nanometer resolution. *Phys Rev Lett* 93:180801. doi:[10.1103/PhysRevLett.93.180801](https://doi.org/10.1103/PhysRevLett.93.180801)
8. Lessard G (2003) Apertureless near-field optical microscopy for fluorescence imaging. Dissertation, California Institute of Technology, Pasadena, CA
9. Hausmann M, Perner B, Rapp A et al (2006) Near-field scanning optical microscopy in cell biology and cytogenetics. *Methods Mol Biol* 319: 275–294. doi:[10.1007/978-1-59259-993-6_14](https://doi.org/10.1007/978-1-59259-993-6_14)

10. Gheber LA, Hwang J, Edidin M (1998) Design and optimization of a near-field scanning optical microscope for imaging biological samples in liquid. *Appl Optics* 37: 3574–3581
11. Hwang J, Gheber LA, Margolis L, Edidin M (1998) Domains in cell plasma membranes investigated by near-field scanning optical microscopy. *Biophys J* 74:2184–2190. doi:[10.1016/S0006-3495\(98\)77927-5](https://doi.org/10.1016/S0006-3495(98)77927-5)
12. Chen Y, Shao L, Ali Z et al (2008) NSOM/QD-based nanoscale immunofluorescence imaging of antigen-specific T-cell receptor responses during an in vivo clonal V γ 2V δ 2 T-cell expansion. *Blood* 111:4220–4232. doi:[10.1182/blood-2007-07-101691](https://doi.org/10.1182/blood-2007-07-101691)
13. Binnig G, Quate C, Gerber C (1986) Atomic force microscope. *Phys Rev Lett* 56:930–933. doi:[10.1103/PhysRevLett.56.930](https://doi.org/10.1103/PhysRevLett.56.930)
14. Müller DJ, Dufrène YF (2011) Atomic force microscopy: a nanoscopic window on the cell surface. *Trends Cell Biol* 21:1–9. doi:[10.1016/j.tcb.2011.04.008](https://doi.org/10.1016/j.tcb.2011.04.008)
15. Rugar D, Hansma P (1990) Atomic force microscopy. *Phys Today* 43:23–30
16. Martin Y, Williams CC, Wickramasinghe HK (1987) Atomic force microscope—force mapping and profiling on a sub 100-Å scale. *J Appl Phys* 61:4723. doi:[10.1063/1.338807](https://doi.org/10.1063/1.338807)
17. Zhong Q, Inniss D, Kjoller K, Elings VB (1993) Fractured polymer/silica fiber surface studied by tapping mode atomic force microscopy. *Surf Sci Lett* 290:L688–L692. doi:[10.1016/0167-2584\(93\)90906-Y](https://doi.org/10.1016/0167-2584(93)90906-Y)
18. Huang L, Su C (2004) A torsional resonance mode AFM for in-plane tip surface interactions. *Ultramicroscopy* 100:277–285. doi:[10.1016/j.ultramic.2003.11.010](https://doi.org/10.1016/j.ultramic.2003.11.010)
19. Schaap IAT, Carrasco C, de Pablo PJ, Schmidt CF (2011) Kinesin walks the line: single motors observed by atomic force microscopy. *Biophys J* 100:2450–2456. doi:[10.1016/j.bpj.2011.04.015](https://doi.org/10.1016/j.bpj.2011.04.015)
20. Sharma S, Grintsevich EE, Phillips ML et al (2011) Atomic force microscopy reveals drebrin induced remodeling of f-actin with sub-nanometer resolution. *Nano Lett* 11:825–827. doi:[10.1021/nl104159v](https://doi.org/10.1021/nl104159v)
21. Dickenson NE, Moore D, Suprenant KA, Dunn RC (2007) Vault ribonucleoprotein particles and the central mass of the nuclear pore complex. *Photochem Photobiol* 83:686–691. doi:[10.1111/j.1751-1097.2007.00050.x](https://doi.org/10.1111/j.1751-1097.2007.00050.x)
22. Quist A, Doudevski I, Lin H et al (2005) Amyloid ion channels: a common structural link for protein-misfolding disease. *Proc Natl Acad Sci U S A* 102:10427–10432. doi:[10.1073/pnas.0502066102](https://doi.org/10.1073/pnas.0502066102)
23. Hinterdorfer P, Dufrène YF (2006) Detection and localization of single molecular recognition events using atomic force microscopy. *Nat Methods* 3:347–355. doi:[10.1038/nmeth871](https://doi.org/10.1038/nmeth871)
24. Bergkvist M, Cady NC (2011) Chemical functionalization and bioconjugation strategies for atomic force microscope cantilevers. *Methods Mol Biol* 751:381–400. doi:[10.1007/978-1-61779-151-2_24](https://doi.org/10.1007/978-1-61779-151-2_24)
25. Roduit C, van der Goot FG, De Los Rios P et al (2008) Elastic membrane heterogeneity of living cells revealed by stiff nanoscale membrane domains. *Biophys J* 94:1521–1532. doi:[10.1529/biophysj.107.112862](https://doi.org/10.1529/biophysj.107.112862)
26. Rief M, Gautel M, Oesterhelt F et al (1997) Reversible unfolding of individual titin immunoglobulin domains by AFM. *Science* 276:1109–1112. doi:[10.1126/science.276.5315.1109](https://doi.org/10.1126/science.276.5315.1109)
27. Linke WA, Grützner A (2007) Pulling single molecules of titin by AFM—recent advances and physiological implications. *Pflugers Arch* 456:101–115. doi:[10.1007/s00424-007-0389-x](https://doi.org/10.1007/s00424-007-0389-x)
28. Axelrod D (1981) Cell-substrate contacts illuminated by total internal reflection fluorescence. *J Cell Biol* 89:141–145. doi:[10.1083/jcb.89.1.141](https://doi.org/10.1083/jcb.89.1.141)
29. Toomre D, Bewersdorf J (2010) A new wave of cellular imaging. *Annu Rev Cell Dev Biol* 26:285–314. doi:[10.1146/annurev-cellbio-100109-104048](https://doi.org/10.1146/annurev-cellbio-100109-104048)
30. Merrifield CJ, Feldman ME, Wan L, Almers W (2002) Imaging actin and dynamin recruitment during invagination of single clathrin-coated pits. *Nat Cell Biol* 4:691–698. doi:[10.1038/ncb837](https://doi.org/10.1038/ncb837)
31. Yildiz A (2003) Myosin V walks hand-over-hand: single fluorophore imaging with 1.5-nm localization. *Science* 300:2061–2065. doi:[10.1126/science.1084398](https://doi.org/10.1126/science.1084398)
32. Saffarian S, Kirchhausen T (2008) Differential evanescence nanometry: live-cell fluorescence measurements with 10-nm axial resolution on the plasma membrane. *Biophys J* 94:2333–2342. doi:[10.1529/biophysj.107.117234](https://doi.org/10.1529/biophysj.107.117234)
33. Karatekin E, Tran VS, Huet S et al (2008) A 20-nm step toward the cell membrane preceding exocytosis may correspond to docking of tethered granules. *Biophys J* 94:2891–2905. doi:[10.1529/biophysj.107.116756](https://doi.org/10.1529/biophysj.107.116756)
34. Minsky M (1961) Microscopy apparatus. US Patent 3,013,467A.
35. Stelzer EHK (1998) Contrast, resolution, pixelation, dynamic range and signal-to-noise ratio: fundamental limits to resolution in fluorescence light microscopy. *J Microsc* 189:15–24. doi:[10.1046/j.1365-2818.1998.00290.x](https://doi.org/10.1046/j.1365-2818.1998.00290.x)
36. Webb RH (1996) Confocal optical microscopy. *Rep Prog Phys* 59:427–471. doi:[10.1088/0034-4885/59/3/003](https://doi.org/10.1088/0034-4885/59/3/003)

37. Cox IJ, Sheppard CJ, Wilson T (1982) Improvement in resolution by nearly confocal microscopy. *Appl Optics* 21:778–781. doi:[10.1364/AO.21.000778](#)
38. Hell SW, Wichmann J (1994) Breaking the diffraction resolution limit by stimulated emission: stimulated-emission-depletion fluorescence microscopy. *Opt Lett* 19:780–782. doi:[10.1364/OL.19.000780](#)
39. Heintzmann R, Cremer CG (1999) Laterally modulated excitation microscopy: improvement of resolution by using a diffraction grating. In: Altschuler GB, Benaron DA, Ehrenberg B et al (eds) SPIE proceedings. SPIE, pp 185–196. doi:[10.1117/12.336833](#)
40. Gustafsson MGL (2005) Nonlinear structured-illumination microscopy: wide-field fluorescence imaging with theoretically unlimited resolution. *Proc Natl Acad Sci U S A* 102:13081–13086. doi:[10.1073/pnas.0406877102](#)
41. Rust MJ, Bates M, Zhuang X (2006) Sub-diffraction-limit imaging by stochastic optical reconstruction microscopy (STORM). *Nat Methods* 3:793–796. doi:[10.1038/nmeth929](#)
42. Betzig E, Patterson GH, Sougrat R et al (2006) Imaging intracellular fluorescent proteins at nanometer resolution. *Science* 313:1642–1645. doi:[10.1126/science.1127344](#)
43. Hess ST, Girirajan TPK, Mason MD (2006) Ultra-high resolution imaging by fluorescence photoactivation localization microscopy. *Biophys J* 91:4258–4272. doi:[10.1529/biophysj.106.091116](#)
44. Hell S, Stelzer EHK (1992) Properties of a 4Pi confocal fluorescence microscope. *J Opt Soc Am A* 9:2159. doi:[10.1364/JOSAA.9.002159](#)
45. Gustafsson MG, Agard DA, Sedat JW (1999) I5M: 3D widefield light microscopy with better than 100 nm axial resolution. *J Microsc* 195:10–16. doi:[10.1046/j.1365-2818.1999.00576.x](#)
46. Gugel H, Bewersdorf J, Jakobs S et al (2004) Cooperative 4Pi excitation and detection yields sevenfold sharper optical sections in live-cell microscopy. *Biophys J* 87:4146–4152. doi:[10.1529/biophysj.104.045815](#)
47. Nagorni M, Hell SW (1998) 4Pi-confocal microscopy provides three-dimensional images of the microtubule network with 100- to 150-nm resolution. *J Struct Biol* 123:236–247. doi:[10.1006/jsbi.1998.4037](#)
48. Lang M, Müller T, Engelhardt J, Hell SW (2007) 4Pi microscopy of type A with 1-photon excitation in biological fluorescence imaging. *Opt Express* 15:2459–2467. doi:[10.1364/OE.15.002459](#)
49. Hell S (1992) Fundamental improvement of resolution with a 4Pi-confocal fluorescence microscope using two-photon excitation. *Opt Commun* 93:277–282
50. Bewersdorf J, Egner A, Hell SW (2006) 4Pi Microscopy. In: Pawley JB (ed) *Handbook of biological confocal microscopy*. Springer, Boston, MA, pp 561–570
51. Denk W, Strickler JH, Webb WW (1990) Two-photon laser scanning fluorescence microscopy. *Science* 248:73–76
52. Hüve J, Wesselmann R, Kahms M, Peters R (2008) 4Pi microscopy of the nuclear pore complex. *Biophys J* 95:877–885. doi:[10.1529/biophysj.107.127449](#)
53. Egner A, Hell SW (2005) Fluorescence microscopy with super-resolved optical sections. *Trends Cell Biol* 15:207–215. doi:[10.1016/j.tcb.2005.02.003](#)
54. Bewersdorf J, Pick R, Hell SW (1998) Multifocal multiphoton microscopy. *Opt Lett* 23:655–657. doi:[10.1364/OL.23.000655](#)
55. Egner A, Andresen V, Hell SW (2002) Comparison of the axial resolution of practical Nipkow-disk confocal fluorescence microscopy with that of multifocal multiphoton microscopy: theory and experiment. *J Microsc* 206:24–32. doi:[10.1046/j.1365-2818.2002.01001.x](#)
56. Egner A, Jakobs S, Hell SW (2002) Fast 100-nm resolution three-dimensional microscope reveals structural plasticity of mitochondria in live yeast. *Proc Natl Acad Sci U S A* 99:3370–3375. doi:[10.1073/pnas.052545099](#)
57. Egner A, Verrier S, Goroshkov A et al (2004) 4Pi-microscopy of the Golgi apparatus in live mammalian cells. *J Struct Biol* 147:70–76. doi:[10.1016/j.jsb.2003.10.006](#)
58. Schmidt R, Wurm CA, Jakobs S et al (2008) Spherical nanosized focal spot unravels the interior of cells. *Nat Methods* 5:539–544. doi:[10.1038/nmeth.1214](#)
59. Gustafsson MGL, Agard DA, Sedat JW (1995) Sevenfold improvement of axial resolution in 3D wide-field microscopy using two objective lenses. In: Wilson T, Cogswell CJ (eds) SPIE proceedings. SPIE, pp 147–156. doi:[10.1117/12.205334](#)
60. Gustafsson MG (1999) Extended resolution fluorescence microscopy. *Curr Opin Struct Biol* 9:627–634. doi:[10.1016/S0959-440X\(99\)00016-0](#)
61. Shao L, Isaac B, Uzawa S et al (2008) I5S: wide-field light microscopy with 100-nm-scale resolution in three dimensions. *Biophys J* 94:4971–4983. doi:[10.1529/biophysj.107.120352](#)
62. Klar TA, Jakobs S, Dyba M et al (2000) Fluorescence microscopy with diffraction resolution barrier broken by stimulated emission. *Proc Natl Acad Sci U S A* 97:8206–8210. doi:[10.1073/pnas.97.15.8206](#)

63. Willig KI, Rizzoli SO, Westphal V et al (2006) STED microscopy reveals that synaptotagmin remains clustered after synaptic vesicle exocytosis. *Nature* 440:935–939. doi:[10.1038/nature04592](https://doi.org/10.1038/nature04592)
64. Hoopmann P, Punge A, Barysch SV et al (2010) Endosomal sorting of readily releasable synaptic vesicles. *Proc Natl Acad Sci U S A* 107:19055–19060. doi:[10.1073/pnas.1007037107](https://doi.org/10.1073/pnas.1007037107)
65. Hell SW (2003) Toward fluorescence nanoscopy. *Nat Biotechnol* 21:1347–1355. doi:[10.1038/nbt895](https://doi.org/10.1038/nbt895)
66. Dyba M, Hell S (2002) Focal spots of size $\lambda/23$ open up far-field fluorescence microscopy at 33 nm axial resolution. *Phys Rev Lett* 88:1–4. doi:[10.1103/PhysRevLett.88.163901](https://doi.org/10.1103/PhysRevLett.88.163901)
67. Westphal V, Hell SW (2005) Nanoscale resolution in the focal plane of an optical microscope. *Phys Rev Lett* 94:143903. doi:[10.1103/PhysRevLett.94.143903](https://doi.org/10.1103/PhysRevLett.94.143903)
68. Abbe E (1873) Beiträge zur Theorie des Mikroskops und der mikroskopischen Wahrnehmung. *Arch Mikrosk Anat* 9:413–418. doi:[10.1007/BF02956173](https://doi.org/10.1007/BF02956173)
69. Kittel RJ, Wichmann C, Rasse TM et al (2006) Bruchpilot promotes active zone assembly, Ca²⁺ channel clustering, and vesicle release. *Science* 312:1051–1054. doi:[10.1126/science.1126308](https://doi.org/10.1126/science.1126308)
70. Willig KI, Kellner RR, Medda R et al (2006) Nanoscale resolution in GFP-based microscopy. *Nat Methods* 3:721–723. doi:[10.1038/nmeth922](https://doi.org/10.1038/nmeth922)
71. Donnert G, Keller J, Wurm CA et al (2007) Two-color far-field fluorescence nanoscopy. *Biophys J* 92:L67–L69. doi:[10.1529/biophysj.107.104497](https://doi.org/10.1529/biophysj.107.104497)
72. Willig KI, Harke B, Medda R, Hell SW (2007) STED microscopy with continuous wave beams. *Nat Methods* 4:915–918. doi:[10.1038/nmeth1108](https://doi.org/10.1038/nmeth1108)
73. Nägerl UV, Willig KI, Hein B et al (2008) Live-cell imaging of dendritic spines by STED microscopy. *Proc Natl Acad Sci U S A* 105:18982–18987. doi:[10.1073/pnas.0810028105](https://doi.org/10.1073/pnas.0810028105)
74. Westphal V, Rizzoli SO, Lauterbach MA et al (2008) Video-rate far-field optical nanoscopy dissects synaptic vesicle movement. *Science* 320:246–249. doi:[10.1126/science.1154228](https://doi.org/10.1126/science.1154228)
75. Kamin D, Lauterbach MA, Westphal V et al (2010) High- and low-mobility stages in the synaptic vesicle cycle. *Biophys J* 99:675–684. doi:[10.1016/j.bpj.2010.04.054](https://doi.org/10.1016/j.bpj.2010.04.054)
76. Watanabe S, Punge A, Hollopeter G et al (2011) Protein localization in electron micrographs using fluorescence nanoscopy. *Nat Methods* 8:80–84. doi:[10.1038/nmeth.1537](https://doi.org/10.1038/nmeth.1537)
77. Rankin BR, Moneron G, Wurm CA et al (2011) Nanoscopy in a living multicellular organism expressing GFP. *Biophys J* 100:L63–L65. doi:[10.1016/j.bpj.2011.05.020](https://doi.org/10.1016/j.bpj.2011.05.020)
78. Berning S, Willig KI, Steffens H et al (2012) Nanoscopy in a living mouse brain. *Science* 335:551. doi:[10.1126/science.1215369](https://doi.org/10.1126/science.1215369)
79. Lichtman JW, Conchello J-A (2005) Fluorescence microscopy. *Nat Methods* 2:910–919. doi:[10.1038/nmeth817](https://doi.org/10.1038/nmeth817)
80. Huang B, Bates M, Zhuang X (2009) Super-resolution fluorescence microscopy. *Annu Rev Biochem* 78:993–1016. doi:[10.1146/annurev.biochem.77.061906.092014](https://doi.org/10.1146/annurev.biochem.77.061906.092014)
81. Fiolka R, Shao L, Rego EH et al (2012) Time-lapse two-color 3D imaging of live cells with doubled resolution using structured illumination. *Proc Natl Acad Sci U S A* 109:5311–5315. doi:[10.1073/pnas.1119262109](https://doi.org/10.1073/pnas.1119262109)
82. Schermelleh L, Heintzmann R, Leonhardt H (2010) A guide to super-resolution fluorescence microscopy. *J Cell Biol* 190:165–175. doi:[10.1083/jcb.201002018](https://doi.org/10.1083/jcb.201002018)
83. Gustafsson MG (2000) Surpassing the lateral resolution limit by a factor of two using structured illumination microscopy. *J Microsc* 198:82–87
84. Heintzmann R, Jovin TM, Cremer C (2002) Saturated patterned excitation microscopy—a concept for optical resolution improvement. *J Opt Soc Am A* 19:1599–1609. doi:[10.1364/JOSAA.19.001599](https://doi.org/10.1364/JOSAA.19.001599)
85. Rego EH, Shao L, Macklin JJ et al (2012) Nonlinear structured-illumination microscopy with a photoswitchable protein reveals cellular structures at 50-nm resolution. *Proc Natl Acad Sci U S A* 109:E135–E143. doi:[10.1073/pnas.1107547108](https://doi.org/10.1073/pnas.1107547108)
86. Gustafsson MGL, Shao L, Carlton PM et al (2008) Three-dimensional resolution doubling in wide-field fluorescence microscopy by structured illumination. *Biophys J* 94:4957–4970. doi:[10.1529/biophysj.107.120345](https://doi.org/10.1529/biophysj.107.120345)
87. Schermelleh L, Carlton PM, Haase S et al (2008) Subdiffraction multicolor imaging of the nuclear periphery with 3D structured illumination microscopy. *Science* 320:1332–1336. doi:[10.1126/science.1156947](https://doi.org/10.1126/science.1156947)
88. York AG, Parekh SH, Dalle Nogare D et al (2012) Resolution doubling in live, multicellular organisms via multifocal structured illumination microscopy. *Nat Methods* 9:749–754. doi:[10.1038/nmeth.2025](https://doi.org/10.1038/nmeth.2025)
89. Thompson RE, Larson DR, Webb WW (2002) Precise nanometer localization analysis for individual fluorescent probes.

- Biophys J 82:2775–2783. doi:[10.1016/S0006-3495\(02\)75618-X](https://doi.org/10.1016/S0006-3495(02)75618-X)
90. Dedecker P, Hofkens J, Hotta J-I (2008) Diffraction-unlimited optical microscopy. *Mater Today* 11:12–21. doi:[10.1016/S1369-7021\(09\)70003-3](https://doi.org/10.1016/S1369-7021(09)70003-3)
 91. Jones SA, Shim S-H, He J, Zhuang X (2011) Fast, three-dimensional super-resolution imaging of live cells. *Nat Methods* 8:499–508. doi:[10.1038/nmeth.1605](https://doi.org/10.1038/nmeth.1605)
 92. Lidke K, Rieger B, Jovin T, Heintzmann R (2005) Superresolution by localization of quantum dots using blinking statistics. *Opt Express* 13:7052–7062. doi:[10.1364/OPEX.13.007052](https://doi.org/10.1364/OPEX.13.007052)
 93. Bobroff N (1986) Position measurement with a resolution and noise-limited instrument. *Rev Sci Instrum* 57:1152. doi:[10.1063/1.1138619](https://doi.org/10.1063/1.1138619)
 94. Bates M, Huang B, Dempsey GT, Zhuang X (2007) Multicolor super-resolution imaging with photo-switchable fluorescent probes. *Science* 317:1749–1753. doi:[10.1126/science.1146598](https://doi.org/10.1126/science.1146598)
 95. Patterson GH, Lippincott-Schwartz J (2002) A photoactivatable GFP for selective photolabeling of proteins and cells. *Science* 297:1873–1877. doi:[10.1126/science.1074952](https://doi.org/10.1126/science.1074952)
 96. Hess ST, Gould TJ, Gudheti MV et al (2007) Dynamic clustered distribution of hemagglutinin resolved at 40 nm in living cell membranes discriminates between raft theories. *Proc Natl Acad Sci U S A* 104:17370–17375. doi:[10.1073/pnas.0708066104](https://doi.org/10.1073/pnas.0708066104)
 97. Greenfield D, McEvoy AL, Shroff H et al (2009) Self-organization of the Escherichia coli chemotaxis network imaged with super-resolution light microscopy. *PLoS Biol* 7:e1000137. doi:[10.1371/journal.pbio.1000137](https://doi.org/10.1371/journal.pbio.1000137)
 98. Manley S, Gillette JM, Patterson GH et al (2008) High-density mapping of single-molecule trajectories with photoactivated localization microscopy. *Nat Methods* 5:155–157. doi:[10.1038/nmeth.1176](https://doi.org/10.1038/nmeth.1176)
 99. Kao HP, Verkman AS (1994) Tracking of single fluorescent particles in three dimensions: use of cylindrical optics to encode particle position. *Biophys J* 67:1291–1300. doi:[10.1016/S0006-3495\(94\)80601-0](https://doi.org/10.1016/S0006-3495(94)80601-0)
 100. Huang B, Wang W, Bates M, Zhuang X (2008) Three-dimensional super-resolution imaging by stochastic optical reconstruction microscopy. *Science* 319:810–813. doi:[10.1126/science.1153529](https://doi.org/10.1126/science.1153529)
 101. Xu K, Zhong G, Zhuang X (2013) Actin, spectrin, and associated proteins form a periodic cytoskeletal structure in axons. *Science* 339:452–456. doi:[10.1126/science.1232251](https://doi.org/10.1126/science.1232251)
 102. Shtengel G, Galbraith JA, Galbraith CG et al (2009) Interferometric fluorescent super-resolution microscopy resolves 3D cellular ultrastructure. *Proc Natl Acad Sci U S A* 106:3125–3130. doi:[10.1073/pnas.0813131106](https://doi.org/10.1073/pnas.0813131106)
 103. Banala S, Maurel D, Manley S, Johnsson K (2012) A caged, localizable rhodamine derivative for superresolution microscopy. *ACS Chem Biol* 7:289–293. doi:[10.1021/cb2002889](https://doi.org/10.1021/cb2002889)
 104. Grimm JB, Sung AJ, Legant WR et al (2013) Carbofluoresceins and carborhodamines as scaffolds for high-contrast fluorogenic probes. *ACS Chem Biol* 8(6):1303–1310. doi:[10.1021/cb4000822](https://doi.org/10.1021/cb4000822)
 105. Lang T, Rizzoli SO (2010) Membrane protein clusters at nanoscale resolution: more than pretty pictures. *Physiology (Bethesda)* 25:116–124. doi:[10.1152/physiol.00044.2009](https://doi.org/10.1152/physiol.00044.2009)
 106. Saka S, Rizzoli SO (2012) Super-resolution imaging prompts re-thinking of cell biology mechanisms: selected cases using stimulated emission depletion microscopy. *Bioessays* 34:386–395. doi:[10.1002/bies.201100080](https://doi.org/10.1002/bies.201100080)
 107. Opazo F, Levy M, Byrom M et al (2012) Aptamers as potential tools for super-resolution microscopy. *Nat Methods* 9:938–939. doi:[10.1038/nmeth.2179](https://doi.org/10.1038/nmeth.2179)
 108. Ries J, Kaplan C, Platonova E et al (2012) A simple, versatile method for GFP-based super-resolution microscopy via nanobodies. *Nat Methods* 9:582–584. doi:[10.1038/nmeth.1991](https://doi.org/10.1038/nmeth.1991)

**Super-Resolution Microscopy Techniques in the
Neurosciences**

Fornasiero, E.; Rizzoli, S. (Eds.)

2014, XVI, 391 p. 130 illus., 116 illus. in color.,
Hardcover

ISBN: 978-1-62703-982-6

A product of Humana Press